AIP Advances

Mitigation of parasitic losses in the quadrupole resonator enabling direct measurements of low residual resistances of SRF samples

Cite as: AIP Advances **11**, 125326 (2021); https://doi.org/10.1063/5.0076715
Submitted: 27 October 2021 • Accepted: 03 December 2021 • Published Online: 27 December 2021

S. Keckert, W. Ackermann, H. De Gersem, et al.

Mitigation of parasitic losses in the quadrupole resonator enabling direct measurements of low residual resistances of SRF samples

Cite as: AIP Advances 11, 125326 (2021); doi: 10.1063/5.0076715
Submitted: 27 October 2021 • Accepted: 3 December 2021 •
Published Online: 27 December 2021

S. Keckert,[1,a] W. Ackermann,[2] H. De Gersem,[2] X. Jiang,[3] A. Ö. Sezgin,[3] M. Vogel,[3] M. Wenskat,[4] R. Kleindienst,[1] J. Knobloch,[1,3] O. Kugeler,[1] and D. Tikhonov[1]

AFFILIATIONS

[1] Helmholtz-Zentrum Berlin, Hahn-Meitner-Platz 1, 14109 Berlin, Germany
[2] Technische Universität Darmstadt, Schloßgartenstraße 8, 64289 Darmstadt, Germany
[3] Universität Siegen, Adolf-Reichwein-Straße 2a, 57076 Siegen, Germany
[4] Universität Hamburg, Mittelweg 177, 20148 Hamburg, Germany

[a] Author to whom correspondence should be addressed: sebastian.keckert@helmholtz-berlin.de

ABSTRACT

The quadrupole resonator (QPR) is a dedicated sample-test cavity for the RF characterization of superconducting samples in a wide temperature, RF field, and frequency range. Its main purpose is high resolution measurements of the surface resistance with direct access to the residual resistance, thanks to the low frequency of the first operating quadrupole mode. In addition to the well-known high resolution of the QPR, a bias of measurement data toward higher values has been observed, especially in higher harmonic quadrupole modes. Numerical studies show that this can be explained by parasitic RF losses on the adapter flange used to mount samples into the QPR. Coating several micrometers of niobium on those surfaces of the stainless steel flange that are exposed to the RF fields significantly reduced this bias, enabling a direct measurement of a residual resistance smaller than 5 nΩ at 2 K and 413 MHz. A constant correction based on simulations was not feasible due to deviations from one measurement to another. However, this issue is resolved given these new results.

I. INTRODUCTION

Superconducting radio frequency (SRF) cavities are a key component for many state-of-the-art particle accelerators. One important figure of merit of such a cavity is its quality factor, determined by its geometry and the material's surface resistance. The surface resistance as a function of RF frequency (f) and temperature (T) is composed of several contributions, commonly approximated as

$$R_S = R_{BCS} + R_{res} = \frac{af^2}{T}\exp\left(-\frac{\Delta}{k_B T}\right) + R_{res}, \quad (1)$$

with R_{BCS} the intrinsic BCS resistance and R_{resthe} residual resistance. Both equations are valid at low fields only and do not contain effects, such as field-dependent losses. R_{BCS} depends on a material parameter (a) and the superconducting energy gap (Δ). The contributions to R_{res} are less well understood and are still under investigation. Hence, for research and development on materials, coatings, or surface treatments aiming at application in SRF cavities, precise measurements of the surface resistance are required.

The quadrupole resonator (QPR) is a dedicated sample-test cavity, providing high resolution measurements in a wide parameter space of temperature and RF field at three different frequencies.[1–4] With a first operating quadrupole mode at about 415 MHz, R_{BCS} at 2 K is typically smaller than 2 nΩ, enabling direct measurements of R_{res}. The operational experience of the QPR indicates a bias of measurement data toward systematically overestimated R_S, limiting the measurement accuracy at low R_S and hence especially impacting R_{res}.[5–7] As an example, Fig. 1 shows a series of measurements of R_S vs temperature for different Nb on copper films and for a bulk Nb sample (JN5). The results show that in the first quadrupole mode ($f \approx 415$MHz), R_{res} is larger than 20 nΩ, even for the bulk niobium sample.

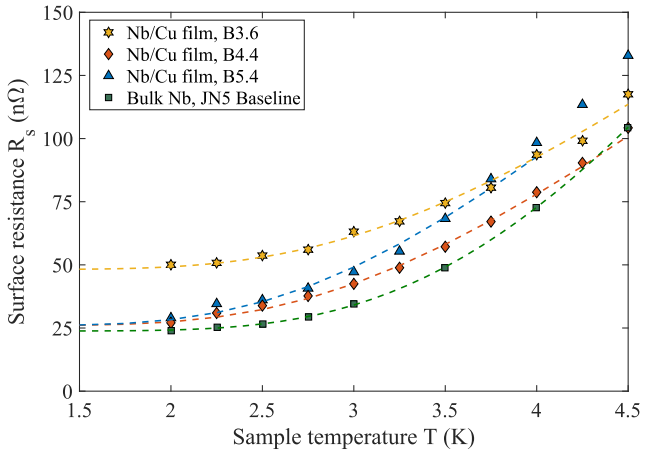

FIG. 1. Representative measurement results for different niobium samples on copper films and for a bulk Nb sample at 415 MHz. The BCS resistance is fitted using Eq. (1).

The QPR uses a calorimetric compensation technique to derive the surface resistance of the sample of interest. First, the sample is heated to a temperature of interest without the RF field, and in thermal equilibrium, the required heater power is recorded. Then, the RF is switched on to the field amplitude of interest. A control loop reduces the DC heater power to reach again and stabilize the temperature of interest. In thermal equilibrium, the RF dissipated power is given by the difference of heater power, allowing us to calculate the surface resistance according to

$$R_S = \frac{2P_{\mathrm{diss}}}{\int_{\mathrm{sample}} \|H\|^2 \mathrm{d}S} = 2c\frac{\Delta P_{\mathrm{DC}}}{P_t Q_t}, \tag{2}$$

with the transmitted power P_t measured at the pickup antenna with coupling Q_t. The calibration constant c is known from simulations, giving the ratio of stored energy to the integral of the RF field on the sample surface. With this calorimetric compensation technique, any heating occurring in the thermal system of the sample assembly is interpreted as the surface resistance of the sample.

In the further course of this paper, we show that the observed behavior of biased residual resistance can be explained by parasitic losses on normal conducting parts of the sample chamber assembly. We provide measurement data of a niobium film sample tested first using a standard stainless steel adapter flange and exhibiting a residual resistance of about 29 nΩ in the first quadrupole mode. The situation is exacerbated at 1.3 GHz due to a reduced damping in the coaxial gap, and a measurement of the residual resistance hitherto was impossible.

Applying a superconducting coating to the flange surfaces that are exposed to (small) RF fields yielded a R_{res} value of less than 5 nΩ. For the first time, QPR measurements at a frequency near 1.3 GHz gave $R_S < 35$ nΩ, enabling us to investigate the frequency-dependent residual resistance. The observed reduction of measured R_S is in good agreement with numerical simulations, proving a significant suppression of the bias and boosting the accuracy of measurement data to an unprecedented level.

II. NUMERICAL ANALYSIS OF PARASITIC LOSSES

In the following, the QPR design is described only briefly. For further details, the reader is referred to Ref. 4. The QPR sample chamber assembly consists of a top-hat-shaped superconducting part and a stainless steel adapter flange as shown in Fig. 2.

The cylindrical sidewall of the inner part is manufactured of high RRR bulk niobium. For research and development on thin films, the top disk acting as a substrate and carrying the sample surface is either built from bulk niobium or copper. The inner part and adapter flange are detachable. An indium wire provides the vacuum seal separating the inner insulation vacuum of the sample chamber from the resonator volume. The assembled sample chamber is inserted into the QPR from below, acting as an inner conductor of a coaxial line as illustrated in Fig. 2. Note that all flanges are made from stainless steel, and the flange on the QPR was brazed to the niobium cavity.

Within the entire resonating structure, a particular mode has to be excited such that a high magnetic field strength will be available on the surface of the sample. For this purpose, a dedicated input coupler is mounted at the ceiling of the resonator where an external power source can be connected. Due to the structural design of the internal system with four rods and two horse-shoe interconnects, a quadrupole mode resonating at ~431.7 MHz serves as the lowest-order mode. The corresponding higher-order modes with repetitive fields along the rods then oscillate at 868.9 MHz and at 1311.7 MHz with nearly identical fields in the vicinity of the sample surface. In particular, the first and last mentioned modes are of interest for many international cavity-design projects because of the proximity to their operational frequencies. Recognizable variations between the measured and simulated frequencies can be attributed to an idealized numerical model. In this study, all numerical simulations have been performed with the help of the CST Studio Suite.[8]

Unfortunately, the desired high magnetic field strength at the top of the sample surface comes together with high magnetic fields in the gap between the sample holder and the lower part of the cavity. This oscillating high magnetic field will subsequently induce related surface currents that will heat up the surface according to the deposited power. In order to attenuate this parasitic electromagnetic

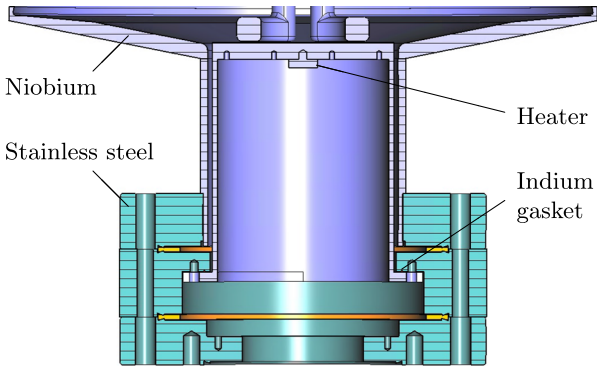

FIG. 2. Cross section of the sample chamber assembly mounted into the lower part of the QPR. The actual sample surface is given by the circular top area positioned at a close distance to the QPR pole shoes. A heater and several temperature sensors (not depicted) are positioned underneath the surface of the sample.

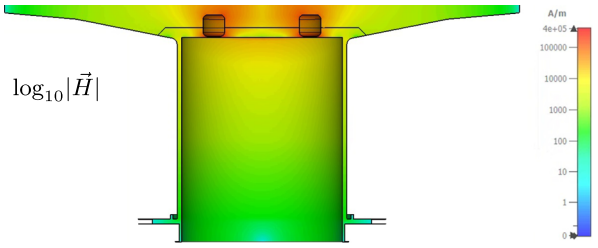

FIG. 3. Simulated distribution of the magnetic field strength in a cross section of the lower part of the QPR.

field within the coaxial structure, the relevant waveguide modes have to be excited below their cutoff frequencies such that they exponentially decay toward the end of the line. For the first relevant quadrupole mode in the cavity, the simulated magnetic field strength is displayed in the vicinity of the sample surface and in the coaxial gap in Fig. 3. Here, a logarithmic scaling is used to demonstrate the deep penetration into the coaxial line.

According to the simulated magnetic field strength, an unavoidable surface current will be induced on the cylindrical walls of the coaxial line and on the stainless steel flanges, as well as on the copper and indium seals. To estimate the contribution of the parasitic heating originating merely from the mounting of the probe into the resonator, the electrical conductivity of niobium at cryogenic temperatures is assumed to be infinitely high compared to the finite values of the surrounding materials specified by $\sigma_{\text{Copper}} = 3.3 \times 10^9 \text{S/m}$, $\sigma_{\text{Indium}} = 3.6 \times 10^8 \text{S/m}$, and $\sigma_{\text{Steel}} = 1.8 \times 10^6 \text{S/m}$.[9] The induced surface current density acting on a material with a finite electrical conductivity will result in a surface power density that will finally locally heat up the field-exposed components to possibly unacceptable temperatures. The simulated distribution of the surface power density on the sample adapter flange is visualized in Fig. 4, where the scaling of the field is chosen such that the total stored energy in the system is 1 J.

The unwanted quadrupolar-like power-density distribution on the surface of the flange naturally originates from the operating quadrupole mode within the QPR. This parasitic power density is numerically determined with the help of eigenvalue calculations and has to be scaled accordingly within the subsequent thermal calculations where different magnetic field amplitudes have to be considered.

Due to the nonlinear thermal behavior of the underlying materials, the simulation of the steady-state temperature distribution has to be restarted again and again once the magnitude of the excitation has changed. A feedback loop back to the eigenvalue solver is not required because the electric conductivities of the applied materials are considered to be constant in the occurring temperature range. The thermal conductivities of the involved materials are taken from Refs. 10 and 11. Thermal boundary resistances between the different parts of the sample chamber are neglected. Earlier work showed that measurement data can be reproduced successfully in simulations with volumetric thermal conductivities only.[6]

For a given field intensity, the calculated temperature distribution in the vicinity of the sample and the flanges is visualized in Fig. 5. Here, the cut plane is chosen such that the hot spots of the temperature due to the quadrupolar excitation become apparent. The highest temperatures naturally arise where the power density is maximal and decrease toward the background, which is modeled by defining a fixed-temperature boundary condition of 2 K. During operation, the entire system is immersed in a bath of superfluid helium, which perfectly justifies the assumed numerical isothermal boundary condition. On account of the fact that the thermal conductivity of niobium is much higher than that of stainless steel, the entire inner cylinder exhibits a nearly constant temperature. Since this sample temperature is determined not only by the applied RF field but also by the chosen geometries and materials, the temperature value itself is not a representative measure to compare different flange designs.

For this reason, additional thermal calculations with various power excitations on a dedicated heater underneath the sample surface have been accomplished, translating the calorimetric RF-DC compensation technique into numerical simulations. The resulting sample temperatures as a function of the excitation power can then reliably be used to specify an effective sample heating power to each simulated sample temperature independent of the actual heat source. In Fig. 6, the result of one of those calculations is visualized where the power is incorporated into the model by a dedicated volumetric heating device underneath the probe.

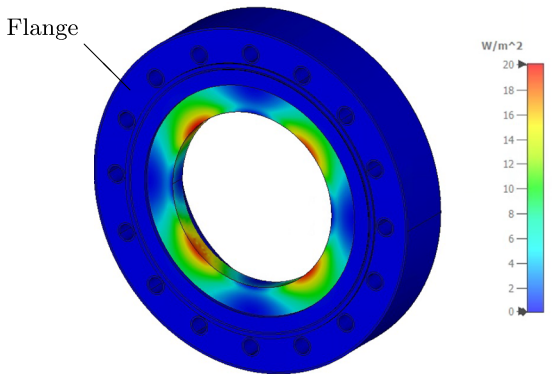

FIG. 4. Simulated distribution of the surface power density on the flange associated with the sample.

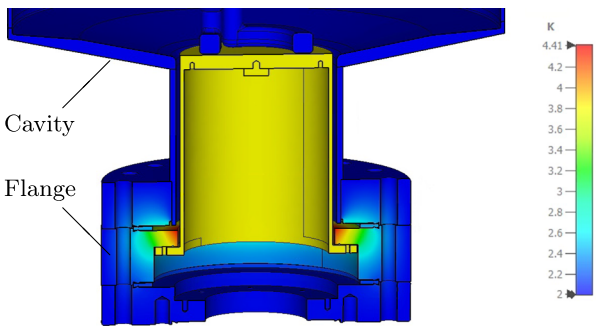

FIG. 5. Simulated temperature distribution due to power dissipation on finite electrical conductive materials (stainless steel flanges and the copper and indium seals) in the lower part of the QPR.

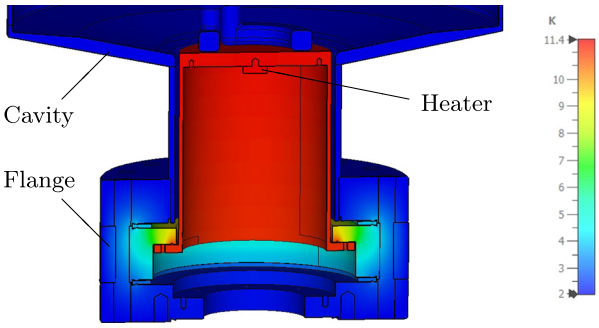

FIG. 6. Simulated temperature distribution in the lower part of the QPR based on an intentional power insertion using a dedicated heater underneath the sample.

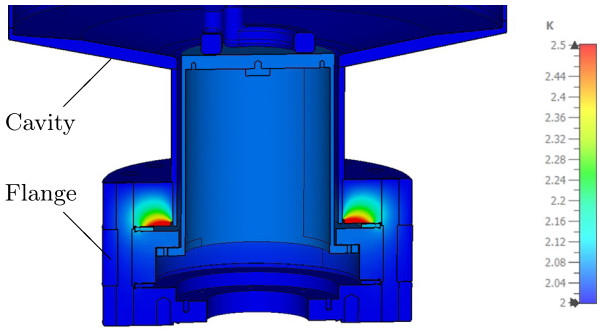

FIG. 7. Simulated temperature distribution due to power dissipation in finite electric conductive materials. The surface of the middle flange corresponding to the mounting of the sample has been coated with niobium.

Following this idea, a series of such calculations do not only enable to assign an effective sample heating power to each calculated steady-state sample temperature, it also allows us to quantify the influence of the artificial heating in terms of an additional surface resistance originating from parasitic heating effects.

In a parametric study, a number of thermal calculations have been performed where the magnitude of the RF field within the QPR has been varied. The results of the comprehensive simulation campaign are summarized in Table I. In this setup, the external heater is not used to heat up the probe in advance to a predefined temperature level. The required electromagnetic field distribution is obtained with the help of a numerical eigenmode calculation where the calculated fields are scaled such that the specified maximum magnetic flux densities on the sample surface are reached. A subsequent thermal calculation with the respective RF heat source thus results in a specific sample temperature, which is specified in Table I for each excitation magnitude individually. By means of separate calculations, the transition from the obtained temperatures to effective powers or even further to parasitic surface resistances is given conclusively for the first three usable quadrupole modes Q_1 to Q_3.

Detailed numerical simulations with normal conductive stainless steel flanges indicate that the unacceptable heating of the sample is mainly attributed to the adapter flange of the sample as can be observed from the temperature distribution visualized in Fig. 5. For this reason, a similar scenario with a modified flange has been investigated. The undesired occurrence of surface heating is prevented by niobium sputtered on the field-exposed surfaces. In the numerical model, the electric conductivity is assumed to reach infinity, while the thermal conductivity of stainless steel remains unchanged. Compared to the results with the normal conductive flanges, the temperature distribution of the modified setup is visualized in Fig. 7. Here, one can clearly see the absence of the strong sample heating, while the remaining heating of the upper flange and both seals are still present. The numerical results of the entire simulation cycle are summarized in Table II.

III. SAMPLE PREPARATION AND FLANGE COATING

The sample tested in this study is a so-called niobium thick film on copper. A sample was coated with 45 μm of niobium using DC magnetron sputtering on a bulk copper substrate at INFN Legnaro.[12] The copper surface was prepared by electropolishing, and then, the niobium film was sputtered in multiple layers (80×500 nm^2 and a top layer of 5 μm).

The adapter flange used to mount the sample into the QPR is a double-side CF100 flange from the 1.442 9-ESU (316LN ESR) material. Prior to the coating, the flange was cleaned in an ultrasonic bath for 10 min. The bath was a water-based solution of sodium hydroxide, 1-propanol, and di-sodium tetraborate decahydrate. After rinsing with deionized water, the flange was dry blown with nitrogen and directly installed into the coating chamber. On the sample holder, the flange was treated with a nitrogen ion-gun and the surface was carefully inspected to be dust free. To protect the CF flange's knife

TABLE I. Sample temperature, effective power, and parasitic surface resistance for the first three quadrupole modes of the QPR resulting from the finite conductivity of the applied materials.

	Q_1			Q_2			Q_3		
B (mT)	T (K)	P (mW)	R_S (nΩ)	T (K)	P (mW)	R_S (nΩ)	T (K)	P (mW)	R_S (nΩ)
5	2.008	0.067	12.6	2.015	0.129	26.0	2.032	0.282	63.1
10	2.030	0.266	12.6	2.058	0.515	26.0	2.124	1.127	63.0
20	2.117	1.062	12.6	2.219	2.050	25.9	2.446	4.449	62.1
50	2.621	6.527	12.4	3.059	12.84	25.9	3.879	30.08	67.3
100	3.803	28.17	13.4	4.801	58.56	29.5	6.513	131.6	73.6

TABLE II. Sample temperature, effective power, and parasitic surface resistance for the first three quadrupole modes of the QPR resulting from the finite conductivity of the applied materials. The sample adapter flange has been coated with niobium.

	Q_1			Q_2			Q_3		
B (mT)	T (K)	P (mW)	R_S (nΩ)	T (K)	P (mW)	R_S (nΩ)	T (K)	P (mW)	R_S (nΩ)
5	2.000	0.001	0.26	2.000	0.003	0.54	2.001	0.006	1.36
10	2.001	0.005	0.26	2.001	0.011	0.54	2.003	0.024	1.36
20	2.002	0.022	0.26	2.005	0.043	0.54	2.011	0.097	1.36
50	2.016	0.136	0.26	2.030	0.269	0.54	2.068	0.606	1.35
100	2.061	0.544	0.26	2.118	1.071	0.54	2.255	2.408	1.35

edge from coating, the area was covered by a metal ring. This prevents possible particulate creation during the subsequent mounting into the resonator due to the potential delamination of the coating from the CF knife edge.

After a bakeout at 650 °C for 5 h, the base pressure of the coating system dropped to 1×10^{-7} mbar. The flange was coated by high power impulse magnetron sputtering (HiPIMS) in an Ar atmosphere with a process pressure of 2.3×10^{-2} mbar, a temperature of 400 °C, a target power of 600 W, and a sample bias of −50 V DC. The target was made of a 90×100 mm^2 RRR 300 grade niobium plate. During coating, the flange was continuously moved bidirectionally (rocking) in front of the target to enhance coating thickness uniformity. The coating process was separated into two parts: beginning with a 1.5-h coating and resulting in a 4 μm thick film, followed by 13 h break under vacuum. The second coating run started with an annealing at 650 °C for 5 h, followed by 3 h of coating. The resultant niobium coating thickness is ~12 μm. After cooling down, the CF knife edge cover and successively the flange was removed from the machine, inspected optically, packed in standard flange covers, and finally sent to be installed into the QPR.

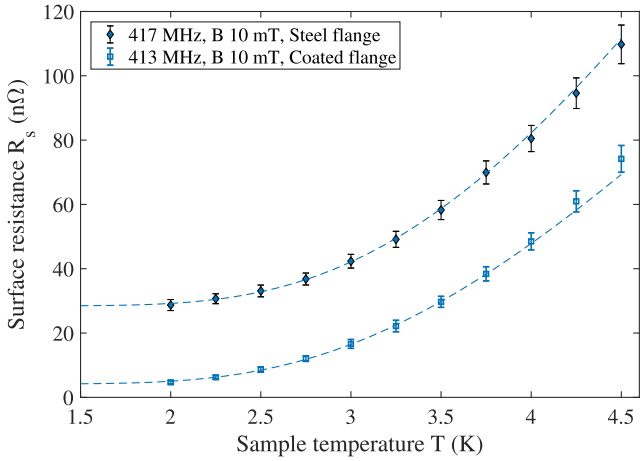

FIG. 8. Measured R_S vs sample temperature at the first quadrupole mode for the baseline and the Nb coated flange test. R_{res} is extrapolated from fits using Eq. (1). The error bars represent the combination of systematic error due to RF calibration only with the statistical error due to cryogenic fluctuations and microphonics.

IV. SURFACE RESISTANCE MEASUREMENTS

Prior to coating the adapter flange, a baseline test of the sample is conducted. Measurement data are shown in Figs. 8 and 9 together with the data of the coated flange. For data taken at a constant level of the RF field (see Fig. 8), R_{res} is extrapolated using Eq. (1). The fit results for the baseline measurement and the test with niobium coated flange are given in Table III. Note that thanks to the low frequency of about 415 MHz and sample temperatures down to 2 K, the uncertainty in R_{res} is less than 1 nΩ. The measured values for R_S of about 25–30 nΩ at the first quadrupole mode near 415 MHz are typical values, also compared to other samples (see Fig. 1).

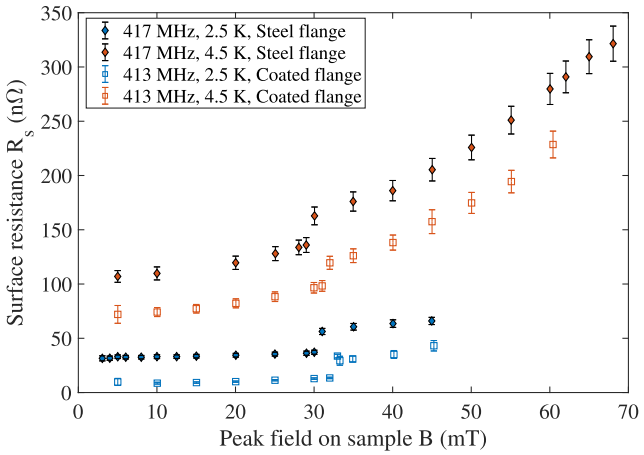

FIG. 9. Surface resistance vs RF field results for the baseline and the Nb coated flange test at different temperatures.

TABLE III. Residual resistance obtained from fitting and selected R_S measurement data at 2.0 and 4.5 K. For all data given, here a constant RF field level of 10 mT was applied.

Setup	Frequency (MHz)	R_S at 2.0 K (nΩ)	R_S at 4.5 K (nΩ)	R_{res} (nΩ)
Baseline	413	28.7	110	28.5
Niobium	417	4.7	74.2	4.2
Coated	844	15.2	284	13.1
Flange	1285	33.8	696	31.6

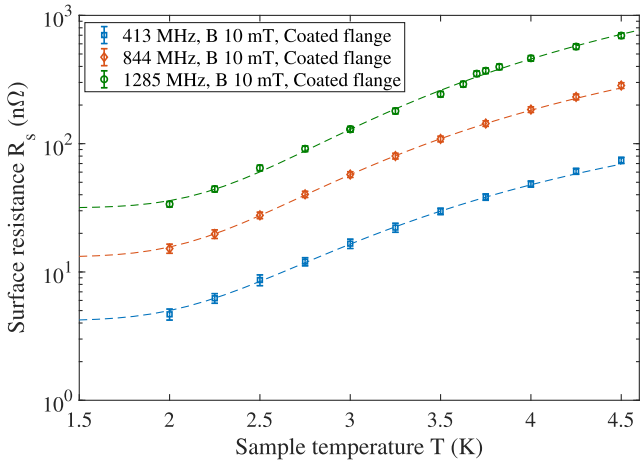

FIG. 10. Measured R_S vs sample temperature for all three quadrupole modes, all measured with the niobium coated flange at 10 mT. R_{res} is extrapolated from fits using Eq. (1).

Measured surface resistance vs RF field at constant temperature shows a "jump" in R_S at about 30 mT (see Fig. 9). The field level at which the jump occurs depends weakly on temperature, while the amplitude remains constant. This can be interpreted as a "Q-switch" behavior of the sample, independent of the adapter flange.[13] The visible "jump" in R_S data at the same field level and with the same amplitude for the baseline and Nb coated flange test excludes significant errors coming from the RF measurements or possible mounting issues.

Thanks to the strong suppression of RF dissipation on the niobium coated adapter flange, especially at higher frequencies, the measurements of R_S were possible at all three quadrupole modes at temperatures down to 2 K. Measurement data together with fits extrapolating R_{res} according to Eq. (1) are shown in Fig. 10.

V. DISCUSSION

The presented measurements clearly show that the application of a superconducting niobium coating on the stainless steel adapter flange at the far end of the coaxial gap between the quadrupole resonator and the QPR sample solved the problem with systematic errors from which the QPR suffered in the past. The surface resistance vs temperature measurement of the first quadrupole mode with the Nb-coated adapter flange (see Fig. 8) shows a reduction by 24 nΩ over the entire temperature range. The numerical simulations predicted only 12.6 nΩ for this mode (see Table I); however, the simulation was performed with an idealized geometry and without allowing for geometrical tolerances. The difference might stem from such deviations, for example, from coaxiality or co-planarity between pole-shoes and sample. They result in a larger fraction of dipole mode or even give rise to a monopole mode to propagate through the coaxial gap reaching the bottom flange. The obtained results suggest that such conceivable problems were also solved by coating the adapter flange with niobium.

The measured R_S values are now comparable with those obtained in SRF cavity measurements. Until now, no sample-test cavity has demonstrated absolute R_S values lower than 5 nΩ. The measurements of R_S as a function of the RF magnetic field show that the error in R_S—originating from parasitic losses in the stainless steel adapter flange—is nearly independent of temperature and applied RF field strength (see Fig. 9). This was expected from the numerical simulations because the dissipated power depends quadratically on the RF field amplitude for both superconductors and normal conductors. Hence, the contribution of parasitic losses to the observed R_S mainly affects the measurement accuracy of R_{res} and can be treated as a systematic bias. On a side note, the measurement precision, i.e., the reproducibility of a measurement, has always been very good and was not further improved by the flange coating. It is conceivable that a dependence on temperature or RF field amplitude could originate from temperature dependent thermal conductivities; however, this would only be a second-order effect and could not explain the measured data.

Looking at the simulation results for the third quadrupole mode (Q3) in the case of normal conducting adapter flange sheds light on the question of a temperature dependent bias from parasitic losses (see Table I). Increasing the RF field amplitude up to 100 mT, which is close to the quench limit of the QPR, leads to an increased bias of 74 nΩ, compared to 63 nΩ at a low field. This difference of about 11 nΩ corresponds to a sample temperature of 6.5 K as opposed to 2 K at a low field. Hence, when extracting BCS parameters for niobium at temperatures up to 4.5 K, the temperature dependent component of the bias will be smaller than 11 nΩ. Due to the strong increase of R_{BCS} with temperature and a minimum RF measurement uncertainty of about 5%, BCS fit results will not be affected significantly by a possibly temperature dependent bias.

Unfortunately, baseline data for this sample are not available at higher harmonic quadrupole modes. However, operational experience indicates that the reduction of the measured R_S value is significantly higher at higher frequencies. Especially at the third mode, R_{res} has never been lower than several hundred nano-ohms. Here, the absolute numbers of expected R_S bias from parasitic heating as obtained from the numerical simulations seem low. Analogous to the considerations of the first quadrupole mode, this might be due to dipole mode components of the RF field penetrating the coaxial structure and heating a normal conducting flange. Simulations investigating this effect are ongoing, and the first results show that indeed manufacturing tolerances and geometrical imperfections lead to an increased level of the RF field at the end of the coaxial structure. This would lead to additional parasitic heating that is not considered in the simulations discussed here and is also prevented by the niobium coating of the flange. Specifically, dipole components at the third quadrupole mode excited above the dipole cutoff frequency would cause a significant contribution when dissipating on normal conducting surfaces.

VI. SUMMARY

In this paper, we presented an extensive numerical study quantifying the impact of parasitic losses at the normal conducting adapter flange for QPR measurements together with experimental data. These parasitic losses cause a systematic bias of surface resistance measurement data, mainly affecting the extracted residual resistance. Coating those areas of the stainless steel flange that are exposed to RF fields with several micrometers of niobium leads to a very effective suppression of this bias.

Measurements with a niobium thick-film sample before and after coating the adapter flange showed a reduction of measured surface resistance by 24 nΩ at the first quadrupole mode. While it depends only weakly on temperature and the RF field amplitude, there is a strong frequency dependence. At the third quadrupole mode, surface resistance values lower than 35 nΩ have been achieved, boosting the accuracy of the measurement system to an unprecedented level. A reduction of measured surface resistance that is larger than that predicted from simulations is attributed to the additional suppression of RF losses from dipole mode components of the RF field. Further simulations investigating the amplitude of possible dipole mode contributions are ongoing. Establishing coated flanges as a new standard for QPR samples opens up new possibilities for the RF characterization of superconducting samples, e.g., investigating the frequency-dependent residual resistance.

ACKNOWLEDGMENTS

We thank V. Garcia Diaz, E. Chyhyrynets, and C. Pira (INFN Legnaro, Italy) for supplying the niobium thick-film QPR sample which has received funding from the European Union's Horizon 2020 Research and Innovation program under Grant Agreement No. 101004730.

We would like to express our gratitude to the SMART collaboration—coordinated by the spokesperson W. Hillert (Universität Hamburg)—for many fruitful discussions. This research was funded by the Federal Ministry of Education and Research of Germany (BMBF) (Project No. 05K2019-SMART).

AUTHOR DECLARATIONS

Conflict of Interest

The authors have no conflicts of interest to disclose.

DATA AVAILABILITY

The data that support the findings of this study are available from the corresponding author upon reasonable request.

REFERENCES

[1] E. Chiaveri, E. Haebel, E. Mahner, and J. M. Tessier, "The quadrupole resonator, construction, RF system, field calculations and first applications," in *Proceedings of the 6th European Particle Accelerator Conference (EPAC'98)* (IOP Publishing, Stockholm, Sweden, 1998), pp. 1852–1854.

[2] E. Mahner, S. Calatroni, E. Chiaveri, E. Haebel, and J. M. Tessier, "A new instrument to measure the surface resistance of superconducting samples at 400 MHz," Rev. Sci. Instrum. **74**, 3390–3394 (2003).

[3] T. Junginger, W. Weingarten, and C. Welsch, "Extension of the measurement capabilities of the quadrupole resonator," Rev. Sci. Instrum. **83**, 063902 (2012).

[4] S. Keckert, R. Kleindienst, O. Kugeler, D. Tikhonov, and J. Knobloch, "Characterizing materials for superconducting radiofrequency applications—A comprehensive overview of the quadrupole resonator design and measurement capabilities," Rev. Sci. Instrum. **92**, 064710 (2021).

[5] R. Kleindienst, "Radio frequency characterization of superconductors for particle accelerators," Dr. rer. nat. dissertation (Universität Siegen, 2017).

[6] S. Keckert, "Characterization of Nb_3Sn and multilayer thin films for SRF applications," Dr. rer. nat. dissertation (Universität Siegen, 2019).

[7] S. Keckert, T. Junginger, J. Knobloch, and O. Kugeler, "The challenge to measure nanoohm surface resistance on SRF samples," in *Proceedings of the 9th International Particle Accelerator Conference, Vancouver, BC, Canada, 29 April–4 May 2018* (IOP Publishing, 2018), pp. 2812–2815.

[8] Dassault Systèmes, "CST Studio Suite."

[9] M. Merio, "Material properties for engineering analysis of SRF cavities," Technical Report No. ED0371110, Fermilab Technical Division Department Rev. A, Batavia, IL, 2013, 5500.000-ES-371110.

[10] F. Koechlin and B. Bonin, "Parametrization of the niobium thermal conductivity in the superconducting state," Supercond. Sci. Technol. **9**, 453–460 (1996).

[11] NIST Standard Reference Data Project, National Institute of Standards and Technology, https://trc.nist.gov/cryogenics/index.html.

[12] V. Garcia Diaz, O. Azzolini, E. Chyhyrynets, G. Keppel, F. Stivanello, M. Zanierato, C. Pira, D. Fonnesu, O. Kugeler, D. Tikhonov, R. Valizadeh, and M. Vogel, "Thick film morphology and sc characterizations of 6 GHz Nb/Cu cavities," in Proceedings of the 2021 International Conference on RF Superconductivity (SRF'21), 2021.

[13] H. Padamsee, J. Knobloch, and T. Hays, *RF Superconductivity for Accelerators*, 2nd ed. (Wiley, 2008).